LA-UR- 96-2008

CONF-9606253--1

Title: AN EXAMPLE OF USING OIL-PRODUCING INDUCED MICROSEISMICITY IN CHARACTERIZING A NATURALLY FRACTURED RESERVOIR

Author(s): James T. Rutledge, W. Scott Phillips (Nambe Geophysical)
Barbra K. Schuessler, David W. Anderson (EES-4)

Submitted to: 6th CONFERENCE ON ACOUSTIC EMISSION/MICROSEISMIC ACTIVITY IN GEOLOGIC STRUCTURES AND MATERIALS
THE PENN. STATE UNIV., JUNE 11-13, 1996

Los Alamos
NATIONAL LABORATORY

Form No. 836 R5
ST 2629 10/91

AN EXAMPLE OF USING OIL-PRODUCTION INDUCED MICROSEISMICITY IN CHARACTERIZING A NATURALLY FRACTURED RESERVOIR

James T. Rutledge and W. Scott Phillips
Nambe Geophysical, Inc.
Route 1 Box 104F, Santa Fe, NM 87501

Barbra K. Schuessler and David W. Anderson
Los Alamos National Laboratory
GeoEngineering Group, MS D443, Los Alamos, NM 87545

ABSTRACT

Microseismic monitoring was conducted using downhole geophone tools deployed in the Seventy-Six oil field, Clinton County, Kentucky. Over a 7-month monitoring period, 3237 microearthquakes were detected during primary oil production; no injection operations were conducted. Gross changes in production rate correlate with microearthquake event rate with event rate lagging production-rate changes by about 2 weeks. Hypocenters and first-motion data have revealed low-angle, thrust fracture zones above and below the currently drained depth interval. Production history, well logs and drill tests indicate the seismically-active fractures are previously drained intervals that have subsequently recovered to hydrostatic pressure via brine invasion. The microseismic data have revealed, for the first time, the importance of the low-angle fractures in the storage and production of oil in the study area. The seismic behavior is consistent with poroelastic models that predict slight increases in compressive stress above and below currently drained volumes.

INTRODUCTION

The technique of mapping conductive fractures using induced microseismicity has been demonstrated in several applications of hydraulic fracture operations (e.g. Albright and Pearson, 1982; Fehler et al., 1986; and Keck and Withers, 1994). Induced seismicity has also been associated with subsurface fluid extraction (e.g. Yerkes and Castle, 1976; Segall, 1989; and Grasso and Wittlinger, 1990) and more complex operations involving sequential or simultaneous extraction and pressure recovery operations (e.g. Niitsuma et al., 1987; Davis and Pennington, 1989; and Rutledge et al., 1994a). In this paper we demonstrate an application of mapping natural, conductive reservoir fractures on an interwell scale (100's of meters) using oil production-induced microearthquakes. Three successful monitoring tests were conducted from 1993 to 1995 in a shallow (<500 m) oil field located in Clinton County, Kentucky. Preliminary results of the first two tests revealed low-angle reservoir fractures that were not previously known to exist (Rutledge et al., 1994b). Herein we present the results of the third monitoring test. The new data indicate both temporal and spatial relationships between the microseismicity and production.

BACKGROUND

Potential for high-volume oil production has been demonstrated from shallow oil reservoirs in Clinton County, Kentucky (Figure 1) (Hamilton-Smith et al., 1990). Oil is produced from low porosity (<2%) carbonate rocks of Ordovician age, spanning the section from the Lexington Limestone to the Knox Group, at depths <600 m (Figure 2). Comparted fracture storage and permeability is suggested by isolated, high-volume production wells.

Initial production rates as high as 64 m^3 per hour and cumulative production of 16000 m^3 from a single well have been reported. Sixty-five km west of Clinton County, near Glasgow, Kentucky, narrow trends of synclinal oil production from shallow (135 to 180 m) carbonate reservoirs have been associated with basement-controlled fault structures (Black, 1986a) (Figure 1). The Glasgow reservoirs are restricted to local zones of fractured, dolomitized limestones, interpreted to be related to secondary faults and fractures resulting from right-lateral, strike-slip reactivation of a deeper basement fault. Similar basement-controlled Paleozoic structures and associated dolomitization have been identified throughout central Kentucky (Black, 1986b). To our knowledge, no detailed investigations of the reservoir fracture systems have been conducted that would provide further guidance in exploration and field development in central Kentucky.

Our study area comprises a narrow trend of new production along the Indian Creek Syncline extending about 2 km ENE from the Seventy-Six oil field (Figure 1). The Seventy-Six field was developed and abandoned in the late-1940s (Wood, 1948). Production resumed December, 1992 with the completion of the Petro-Hunt # 1 Frank Summers well on the NE margins of the abandoned field (well FS1 of Figure 1). The microearthquakes were detected using downhole geophone tools placed at or near reservoir depth in wells offset 120 to 170 m from a new, high-volume well. Typical high-volume wells in the study area flow to surface for a few days at rates of 80 to 240 m^3 per day and are then put on pump (sucker-rod pump). Cumulative production is on the order of 1600 to 2400 m^3 over periods of 6 to 12 months. Production along the Indian Creek Syncline has been primarily from the middle-Ordovician High Bridge Group (equivalent to the Stones River Group of Tennessee) at depths ranging from about 300 to 460 m (Figure 2). The High Bridge Group consists mainly of argillaceous limestone deposited in a shallow-marine to tidal-flat environment (Gooding et al., 1988).

DATA

Data were collected using downhole, 3-component geophone tools. A mechanical arm couples the instruments to the borehole wall. The tools were equipped with 8 or 30 Hz geophones. Downhole amplification of the geophone outputs was 60 dB. At the surface the data signals are further amplified and anti-alias filtered before input to a triggered, digital, PC-based, data acquisition system. Data were sampled at a 0.2 msec interval per channel.

Monitoring was conducted near the Ohio Kentucky Oil Corporation's #1 Hank Thomas (HT1) production well (Figure 1). Figure 3 shows the cumulative production and event detection during the monitoring period. No injection activity was conducted before or during monitoring. HT1 was completed and put on-line November 27, 1995 (start of week zero, Figure 3). Monitoring started week 6 and terminated at the beginning of week 28 (Figure 3). Two geophones were initially deployed in GT8 at 427 and 244 m depth. A third geophone was placed in BU1 at 396 m depth during week 15 (Figure 1). Figure 4 shows an example of a microearthquake's 3-component waveforms recorded in the study area.

During the monitor period, HT1 production (~1300 m^3) accounted for 97% of the volume extracted in the immediate study area. A total of 3237 microearthquakes were detected. Change in gross production rate correlates with event rate. The event rate lags production rate change by about 2-weeks (Figure 3). Production decline at week 13 is followed by a decrease in event rate at week 15 (trigger criteria was not changed with the ad-

dition of the third tool in well BU1 during week 15). Production records for HT1 after week 22 were not available. We presume production continued to decline from week 22 to 28. HT1 production was terminated during week 28 when the well was deepened using an air-rotary rig. Deepening of HT1 directly connected the original productive interval with a water-filled fracture at hydrostatic pressure (located by production induced seismicity and discussed further below). HT1 was then plugged back to its original total depth (TD) and put back on-line. Production efforts were immediately terminated due to large volumes of water produced from the original production depth which produced no water before deepening (L. Wagoner, Ohio Kentucky Oil Corp., pers. commun., 1995). The presence of water indicated the drained volume was at least partially repressurized via the borehole connection to the deeper fracture. A nearby lightning strike temporarily terminated monitoring at the start of week 28, a few days before HT1 was deepened. Monitoring resumed from weeks ~30^1/2 to 36 (not shown in Figure 3) during which only 2 microearthquakes were detected. In the 3 weeks before the HT1 productive interval was inadvertently repressurized, the event rate was 120 times greater than the subsequent measured rate.

The gross correlation of the production and event rates suggests the observed microearthquakes are triggered by production induced stress changes. After presenting an interpretation of the data below, we discuss the cause/effect relationships and offer some speculation for the 2-week response time.

LOCATING THE MICROEARTHQUAKES

A combination of P- and S-wave arrival times and P-wave particle motion trajectories (hodograms) were used to obtain locations since data were collected using only two to three receivers. Arrival times were picked visually and, in general, were very impulsive (Figure 4). Estimated errors in the arrival-time picks were 0.3 msec or less. Azimuthal hodogram data were obtained by eigenvector analysis using the first 2 msec of horizontal-component, P-wave data (Flynn, 1965). Constraints on the directional data (hodograms) were first-arrival signal-to-noise ratio ($\geq$10) and linearity of particle motion (Rutledge et al., 1994b). Velocities were initially determined using sonic logs, and downhole calibration shots, and then using a joint hypocenter-velocity inversion. The downhole calibration shots were also used for determining the orientation of the geophone tools' horizontal components.

The two-station data, in which two receivers were placed in a single borehole 183 m apart, make up the initial 59% of the data collected. Two-station hypocenters were determined in two separate steps, first using the traveltime data to obtain a depth and radial position from the monitor well, and then using the hodogram data to obtain a unique azimuth to the source (Rutledge et al., 1994b). In computing the three-station data hypocenters, traveltime and hodogram data were coupled in an iterative, least-squares computation minimizing the difference between predicted and observed data. Azimuthal hodogram data from the two deeper stations were used (Table 1). These stations had higher signal-to-noise ratios and shorter, lower inclination receiver-source paths. Scaling of traveltimes and angles in units of length was applied to avoid numerical problems with matrix elements differing by orders of magnitude. Data were weighted by the reciprocals of their uncertainties, estimated from residuals of the three station data (Table 1). Location errors are discussed below.

A two-layer velocity model, event locations and the two deep geophone orientations were solved for via a joint hypocenter-velocity inversion. Data used in the inversion were

P-wave arrival times and hodograms from three downhole shots and a subset of the three-station data in which six arrival times (three P and three S) and two hodograms were available (364 events). Parameter separation techniques were used allowing an unlimited number of events to be included in the inversion (Pavlis and Booker, 1980). The boundary between the two layers was kept fixed at the well-defined sonic-velocity boundary at the top of the High Bridge Group (Figure 2). Inclusion of the hodogram data helped resolve trade-off between velocities and hypocenters. In general, the hypocenters aligned in distinct planar clusters (see below). The final velocity model was considered improved from the starting model based on better coplanar alignment of two- and three-station data hypocenters.

Station	P Arrival	S Arrival	Hodogram Azimuth
Well: Depth (m)	(msec)	(msec)	(Degrees)
GT8: 244	0.5	0.1	(not used)
GT8: 427	0.3	0.1	5
BU1: 396	0.3	0.1	4

Table 1: Residual standard deviation of the three-station data

MICROSEISMIC FRACTURE MAPS

Of the 3237 events detected, 1719 were located. A map view is shown in Figure 5. The majority (1548) occur east of well GT3. A cross-section projection of the events located east of GT3, along the profile line C-D of Figure 5, is shown in Figure 6. The microearthquake locations clearly define low-angle planar features. A perspective view of three fracture planes delineated east of GT3 is shown in Figure 7. Grouping into planar clusters was initially accomplished by visual inspection using various 2-dimensional projections and 3-dimensional graphic displays. The planar volumes shown in Figure 7 were then determined from the eigenvectors fitting the distribution of microearthquake locations within each group (Flynn, 1965). Dimensions of the planar volumes exclude 10% of the extreme outer event locations in each dimension, so that outlying hypocenters do not affect the size and shape of the volumes defined by the majority of events. The strike and dip of the planes were determined using the minimum eigenvectors (normals to the planes) (Table 2).

Hypocenter Group	Strike	Dip
Group A	N82°E	17° SE
Group B	N65°E	19° NW
Group C	N67°E	16° SE

Table 2: Orientations of microseismic fracture planes.

Location Errors

Location errors were estimated from residuals of the three-station data (Table 1). The

errors only reflect the station-event geometry, the distribution of data types and data uncertainties; velocity model uncertainties were not considered. Error ellipses in general are linear and trend perpendicular to the event-station direction due to the larger error contribution associated with the hodogram azimuths. Error in depth and radial distance from the monitor boreholes are predominantly associated with the arrival time uncertainties (solely for the two-station locations) and, hence, are smaller. For the two-station event locations, the maximum axis of the error ellipsoids ranged between 10 and 20 m within 250 m of the monitor boreholes, and up to 60 m for the more distant events.The location errors for the three-station data east of GT3 (Figure 5) range between 3 and 5 m. Events that lie on the N-S plane through the two monitor boreholes (GT8 and BU1) have errors up to 20 m and ellipses that are highly linear, trending E-W. Density and temperature logs corroborate the intersection of the seismically-active fractures at wellbores and indicate depth accuracy within 0.5 to 3 m within 200 m of the monitor wells.

Fault Plane Solutions

Composite fault plane solutions were computed for the planar hypocenter groups using the computer program FPFIT (Reasenberg and Oppenheimer, 1985). Figure 8a show the best fit fault plane solutions for the Group B fracture. Groups A and C both dip to the SE and were combined to improve the focal sphere coverage (Figure 8b). First motion data from all receiver tools were used. Orientation of the mapped planes are represented by the dashed curves. P axes are oriented NW-SE at near-horizontal inclination. The composite fault plane solutions indicate a predominantly thrust mechanism; in both cases a pure thrust mechanism can be accommodated within the error of fit. Orientation of the mapped planes are in good agreement with one of the computed nodal planes.

INTERPRETATION

The microearthquakes have revealed a conjugate set of low-angle thrust faults within the productive High Bridge Group formation. These thrust faults strike from N82E to N65E and dip to both the NW and SE at angles ranging from approximately 15° to 20° (Table 2). Below, we summarize the relationship of the seismically-active fractures with respect to production and fluid movement.

The seismically-active fractures: 1) are peripheral to currently drained volumes, 2) have been partially drained by previous production and, 3) have subsequently been resaturated with brine water. While monitoring, 97% of the fluid volume extracted (> 1300 m^3) came from HT1. The seismicity occurs both above and below the production interval of HT1 (Figures 6 and 7) and, in map view, primarily to the west of HT1 (Figure 5). The main seismic zone shown in map view is bounded by older production wells, GT1, GT2, GT3 and GT4 (Figure 5). Production depth intervals of GT1, GT2 and GT4 intersect or align with the seismically-active fractures (Figures 6 and 7). GT4's production intervals intersects the up dip side of the B fracture. GT2's upper production interval intersects the A fracture and its lower production interval, brought on-line after deepening the well, aligns with the C fracture. The productive interval of GT1 aligns with the B fracture's down dip side (Figures 6 and 7). When deepened, GT2 also intersected the up dip side of the B fracture and is corroborated with temperature and neutron porosity log anomalies. GT2 did not produce oil from the B fracture, most likely because of partial drainage already underway from GT1 and GT4. A cumulative oil volume of 725 m^3 was extracted from these 3 wells in the

9 months proceeding monitoring. Only GT1 was on-line with HT1 during monitoring, and it only contributed an additional 25 m^3 of oil. Some water (brine) was also produced from GT1, GT2 and GT4 (water production records were not kept). HT1 produced no water (L. Wagoner, Ohio Kentucky Oil Corp., pers. commun., 1995).

A test well, GT10, was drilled by the Ohio Kentucky Oil Corporation (OKOC) into the lower edge of the group B fracture after 5 months of monitoring (week 28, Figure 3). No fluid was encountered until the drill bit reached the group B fracture at 432 m (Figures 5, 6 and 7). The fracture produced brine water with drill-string air circulation (air-rotary drilling). Drilling was immediately terminated. One week later, OKOC deepened HT1 and also encountered brine water when the well intersected the same group B fracture further up dip at 404 m (Figures 6 and 7). Below, we discuss the source of the brine water.

The oil reservoir in the study area is primarily a set of comparted, low-angle thrust faults. This conclusions follows from the correlation of the older production depth intervals and the low-angle thrust faults mapped using the microseismicity. Logged boreholes intersecting the seismically-active fractures show distinct density and/or temperature anomalies over 1 to 2 m intervals indicating the mapped fractures are characterized as fracture zones 1 to 2 m thick with well developed porosity ranging from about 15 to 35% above baseline values <1%. The density and temperature log anomalies associated with other, seismically-inactive productive fractures are similar in character.

We computed the storage capacity of the group B fracture from the fracture area delineated by the microseismicity and fracture-zone thickness and porosity measured from the log data. The area of the fracture delineated east of GT3 is approximately 300 by 100 m. Assuming 15% porosity developed over a 1 m thick zone gives a volume of 4500 m^3. Productive intervals of GT1 and GT4, which align with the group B fracture zone (Figure 6), produced a cumulative 402 m^3 of oil, implying ~9% oil recovery of original, in-place fluid volume.

The correlation of the event rates and HT1 production strongly suggest that the microseismicity is triggered by the current-production induced stress changes (Figure 3). The spatial correlation of the microseismicity to past production in turn suggests that current drainage follows a similar pattern. Based on these inferences and the similarity of the log responses, we presume that HT1 also produces from a low-angle fracture oriented similar to the adjacent, seismically-active fractures. A plane formed by the productive intervals of HT1, GT3 and a temperature anomaly in GT10, at 354 m, strikes N72°E and dips 22° SE, consistent with the mapped thrust-fault orientations (Table 2 and Figure 7). GT3 was the second, single largest producer in the HT1 monitor area (544 m^3) and also produced at a depth interval between the seismically-active fractures. The inferred fracture would have been partially drained by GT3 before HT1 was drilled and intersected it further down dip (Figure 7). Initial production response supports this interpretation. GT3 initially flowed oil to surface; HT1 did not. Test well GT10 aligns closest with HT1 and GT3 along strike of the microseismic mapped structures. The temperature anomaly in GT10 forms the third point of the plane and is the only significant anomaly on the log. (The group B fracture intersected at GT10's TD could not be spanned by the logging tool.) There is no log evidence of an intermediate-depth fracture zone intersecting the surrounding production wells GT1, GT2 and GT4. Production history also indicates these wells have very poor or no hydraulic conductivity with the volume drained by HT1. Permeability and porosity of the inferred

fracture, therefore, are developed over a narrow zone in the dip direction (<60 m at S18°E). The narrow zone of seismicity extends about 850 m SW of HT1 (Figure 5) suggesting an extensive pressure response in the strike direction. Evidence of immediate pressure communication between wells has been observed in the area at distances greater than 1 km (J.H. Perkins, Petro-Hunt, Inc., pers. commun., 1996).

Historical displacements along the imaged thrust faults are small with vertical throws of about 1 m or less. Detailed log correlations in the area show about 1 m of thickening in section just above a mapped thrust fault (Hamilton-Smith, 1995). The observed thickening could also be due to local infill sedimentation. We can conclude that total historical displacements in dip direction do not exceed about 2 m.

PRESSURE HISTORY

To our knowledge, no reservoir pressure measurements have been made in the area. It has been suggested that the reservoirs are initially overpressured (Hamilton-Smith, et al., 1990; and Hamilton-Smith, 1995). We know that the drained fractures recover to hydrostatic pressure via water invasion (discussed further below). If the reservoir is initially overpressured it implies that a net pore-pressure decrease occurs along fractures from predrainage to subsequent hydrostatic recovery, which would inhibit seismic slip. Therefore, the observed seismic failure along the pressure-cycled fractures suggests the reservoir cannot be overpressured. We assume instead that the reservoirs are initially in equilibrium with far-field pore pressure (hydrostatic) so that little or no net pressure change results from the pressure cycling. Based on field observations of fluid flow, this assumption is not unreasonable.

Initial production in the study is characterized by high-volume flow to the surface. Wells are typically put on pump within a few days of discovery as pressure declines. An overpressured reservoir is not required to flow oil to the surface. Water levels measured in the study area (37 m depth) could support a column of oil (density = 0.82 g/cm^3 (Hamilton-Smith, 1995)) from a production depth of 350 m to 32 m above ground level. Brine in the geologic section and/or gas in the oil would increase the oil's buoyancy.

Wells in the area are configured with casing cemented from the top of the High Bridge Group (about 300 to 350 m depth) to surface and are then completed open hole to TD. Open wellbores intersecting the seismically-active fractures are at local hydrostatic pressure. Well GT2, for example, connects with the seismically-active fractures (Figures 6 and 7) and was water-filled to 37 m depth (250 m elevation). The evidence of water invasion along the previously productive fractures with eventual hydrostatic pressure recovery suggest a natural water drive is active in the area. However, the water drive is very poorly connected to the productive fractures via natural reservoir flow paths and is unable to maintain reservoir pressure during drainage. Pressure decline is evident by the short duration of flow to the surface. Hydraulic isolation of the productive fractures is evident from very low to nonexistent water production during the wells' short productive histories and the highly comparted nature of production from adjacent, sequentially drilled wells. Water invasion and pressure recovery of the drained fractures is facilitated by the open well completions, allowing direct communication between permeable zones at different depths.

DISCUSSION

The temporal correlation of the seismicity and current production rates (Figure 3) sug-

gests the seismicity is induced by production induced stress changes. The 2-week lag time observed between production and event rates may be the response time of pore pressure changes, initially affected at the production wells, to diffuse over some larger area of the fracture currently being drained.

The spatial occurrence of the seismicity is similar to that expected for Segall's (1989) poroelastic stress model. Consistent with the model, slip is inhibited along the currently drained fracture (the inferred, aseismic fracture shown in Figure 7) because the effective stress loading predominantly increases the normal stress across the fracture; slip is triggered on fractures above and below the drained volume (fractures A, B and C of Figure 7) due to small increases in horizontal compression induced by production. Segall (1992) has shown that the magnitude of stress changes outside the reservoir are small relative to pressure decline. At the Lacq gas field, for example, computed poroelastic stress outside the reservoir, where seismicity occurs, was only 0.2 MPa for an observed pressure drop of 60 MPa within the reservoir (Segall et al., 1994). An implication of poroelastic triggered failure, therefore, is that slip is induced on faults already close to failure within the background state of stress. In turn, seismicity would be expected to reflect the background state of stress by exhibiting similar focal mechanism on similarly oriented faults. From our observations, the uniformity of fault orientations and first-motion data are also consistent with poroelastic induced failure (Figure 8).

Previously, Rutledge et al. (1994b) had suggested that the peripheral, seismically-active fractures might be undrained, oil-filled fractures with relatively high pore pressure, in which case, the microseismicity could be used to directly identify offset drilling targets. The drill tests and production histories indicate that the active fractures are at higher pore pressure than the currently drained volumes, but that they have been partially drained and subsequently recovered to hydrostatic pressure via brine invasion. We presume, as discussed above, that initial reservoir pressure was in equilibrium with far-field pore pressure and that little or no net pressure change occurred along the seismically-active fractures from pre-drainage to eventual pressure recovery. In a thrust stress regime, the decrease in Coulomb stress induced along the seismically-active fractures during their prior drainage will be much greater in magnitude than the subsequent increased Coulomb stress resulting from the current, adjacent drainage (Segall and Fitzgerald, 1996). Our assumption of pressure recovery is necessary to bring the previously drained fractures back to a near-critical state of stress in terms of poroelastic triggered failure. The observations of induced slip on the previously drained fractures suggests that the stress path followed during pressure cycling and replacement of oil with brine has resulted in the fractures being more critically stressed than in their pre-drained state.

CONCLUSIONS

Mapping the production-induced microseismicity has revealed previously undetected, conjugate, low-angle fracture sets. The correlation of these fractures with older production intervals and well log porosity anomalies shows that they are the important fractures to find in the exploration and development of the area. The microseismicity only reveals those fractures with a propensity to slip due to their orientation with respect to the current state of stress. Barton et al. (1995) have shown correlations of much higher permeability along fractures oriented optimally for shear failure than fractures less critically stressed in current stress fields. Our study appears to further support that correlation. Surface lineament and

outcrop studies indicate a complex variety of fracture sets in the region (Black, 1986b; and Hamilton-Smith, 1995). Other fracture sets or faults present in the study area may play an important role in comparting the productive, low-angle fractures.

The small-displacement thrust faults pose a difficult exploration problem using conventional seismic reflection data; they are too thin to be imaged directly and do not have enough vertical throw to resolve bedding discontinuities. Consideration of the low-angle fractures as exploration targets will probably require inference from other more mappable subsurface features.

The identification of the productive, low-angle fractures also has implications for field development. Drilling horizontal or deviated wells at these shallow depths does not appear to offer any advantage in increasing the probability of intersecting productive fractures. Dip meter or formation microscanning logs would be useful in determining orientations of low-angle, productive fractures, enabling interwell correlation and mapping of pay zones and further, provide guidance in offset well placement. Interwell correlation and mapping of the conductive fractures will also allow improved planning in plug-and-abandonment operations so as to avoid premature water invasion of pay zones. Pressure maintenance operations could also be attempted once the conductive fracture zones between wells have been mapped.

ACKNOWLEDGMENT

This work was supported by the U.S. Department of Energy's Natural Gas and Oil Technology Partnership. Participants included Los Alamos National Laboratory, the Ohio Kentucky Oil Corporation, Petro-Hunt, Inc., Meridian Exploration Corp. and the Kentucky Geological Survey. We thank James Albright, Bob Hanold, James Drahovzal and Jay Bertram for their efforts in initiating and supporting this study. We thank Don Dreesen for valuable discussions on data interpretation. Special thanks are extended to Tom Fairbanks, Grady Rhodes, Rick Flora, Joel Duran and Steve Harthun for their many hours contributed to field work.

REFERENCES

Albright, J.N. and Pearson, C.F., 1982. Acoustic emissions as a tool for hydraulic fracture location: experience at the Fenton Hill hot dry rock site. Soc. of Petro. Eng. J., 523-530.

Barton, C.A., Zoback, M.D. and Moos, D., 1995. Fluid flow along potentially active faults in crystalline rock. Geology, 23, 683-686.

Black, D.F.B., 1986a. Oil in dolomitized limestone reservoirs in Kentucky. In: M.J. Aldrich, Jr. and A.W. Laughlin (Editors), Proceedings of the 6th International Conference on Basement Tectonics. Int. Basement Tectonics Assoc., Inc., Salt Lake City, Utah.

Black, D.F.B., 1986b. Basement faulting in Kentucky. In: M.J. Aldrich, Jr. and A.W. Laughlin (Editors), Proceedings of the 6th International Conference on Basement Tectonics. Int. Basement Tectonics Assoc., Inc., Salt Lake City, Utah.

Davis, S.D. and Pennington, W.D., 1989. Induced seismic deformation in the Cogdell oil field of west Texas. Bull. Seism. Soc. Am., 79, 1477-1494.

Fehler, M., House L. and Kaieda, H., 1986. Seismic monitoring of hydraulic fracturing: Techniques for determining fluid flow paths and state of stress away from a wellbore.

In: Proc. 27th U.S. Symposium on Rock Mechanics. Tuscaloosa, Alabama, June 23-25.

Flynn, E.A., 1965. Signal analysis using rectilinearity and direction of particle motion. Proc. I.E.E.E., 53, 1725-1743.

Grasso, J.R. and Wittlinger, G., 1990. Ten years of seismic monitoring over a gas field. Bull. Seism. Soc. Am., 80, 450-473.

Hamilton-Smith, T., 1995. Stress, seismicity and structure of shallow fractured carbonate reservoirs of Clinton County, Kentucky.: Final report for Los Alamos National Laboratory: Kentucky Geological Survey Open-File Report, OF-95-02, 143p.

Hamilton-Smith, T., Nuttall, B.C., Gooding, P.J., Walker, D. and Drahovzal, J.A., 1990. High-volume oil discovery in Clinton County, Kentucky. Kentucky Geological Survey, Series 11, Information Circular 33.

Keck, R.G. and Withers, R.J., 1994. A field demonstration of hydraulic fracturing for solid waste injection with real-time passive seismic monitoring. paper SPE 28495, presented at 69th Soc. Petro. Eng. Annual Technical Conference and Exhibition, New Orleans, Louisiana.

Niitsuma, H., Chubachi, N. and Takanohashi, M., 1987. Acoustic emission analysis of a geothermal reservoir and its application to reservoir control. Geothermics, 16, 47-60.

Pavlis, G.L. and Booker, J.R., 1980. The mixed discrete-continuous inverse problem: application to simultaneous determination of earthquake hypocenters and velocity structure. J. Geophys. Res., 85, 4801-4810.

Reasenberg, P. and Oppenheimer, D., 1985. FPFIT, FPPLOT and FPPAGE: Fortran computer programs for calculating and displaying earthquake fault-plane solutions. U.S. Geological Survey, Open-File Report 85-0739.

Rutledge, J.T., Faibanks, T.D., Albright, J.N., Boade, R.R., Dangerfield, J. and Landa, G.H., 1994a. Reservoir seismicity at the Ekofisk oil field. In: Proceedings EUROCK '94, Rock mechanics in petroleum engineering, Soc. Petro. Eng. / Int. Soc. Rock Mech. International Conference, Delft, The Netherlands.

Rutledge, J.T., Phillips, W.S., Roff, A., Albright, J.N., Hamilton-Smith, T., Jones, S.K. and Kimmich, K.C., 1994b. Subsurface fracture mapping using microearthquakes detected during primary oil production, Clinton County, Kentucky. paper SPE 28384, presented at 69th Soc. Petro. Eng. Annual Technical Conference and Exhibition, New Orleans, Louisiana.

Segall, P., 1989. Earthquakes triggered by fluid extraction. Geology, 17, 942-946.

Segall, P., 1992. Induced stresses due to fluid extraction from axisymmetric reservoirs. Pure Appl. Geophys., 139, 535-560.

Segall, P., Grasso, J.R. and Mossop, A., 1994. Poroelastic stressing and induced seismicity near the Lacq gas field, southwestern France. J. Geophys. Res., 99, 15423-15438.

Segall, P. and Fitzgerald, S., 1996. A note on induced stress changes in hydrocarbon and geothermal reservoirs. Tectonophysics (in press).

Wood, E.B., 1948. The Seventy-six oil pool: Kentucky Geological Survey Open-File Re-

port OF-48-01, 10p.

Yerkes, R.F. and Castle, R.O., 1976. Seismicity and faulting attributable to fluid extraction. Eng. Geol., 10, 151-167.

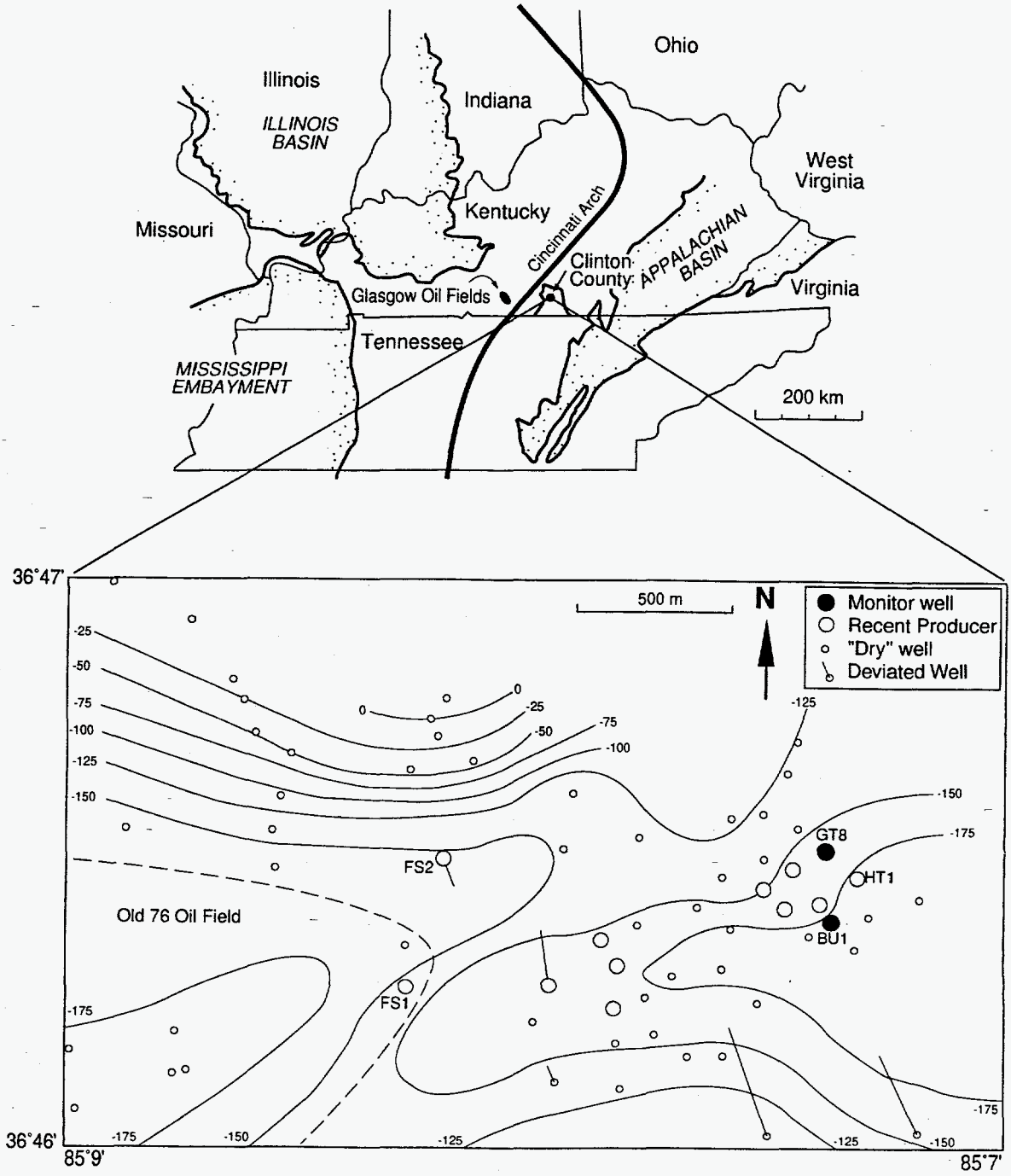
Ohio
Illinois
Indiana
ILLINOIS BASIN
West Virginia
Kentucky
Missouri
Cincinnati Arch
Clinton County
APPALACHIAN BASIN
Virginia
Glasgow Oil Fields
Tennessee
MISSISSIPPI EMBAYMENT
200 km
36°47'
500 m
N
Monitor well
Recent Producer
"Dry" well
Deviated Well
-25
-50
-75
-100
-125
-150
-175
0
FS2
GT8
HT1
BU1
FS1
Old 76 Oil Field
36°46'
85°9'
85°7'

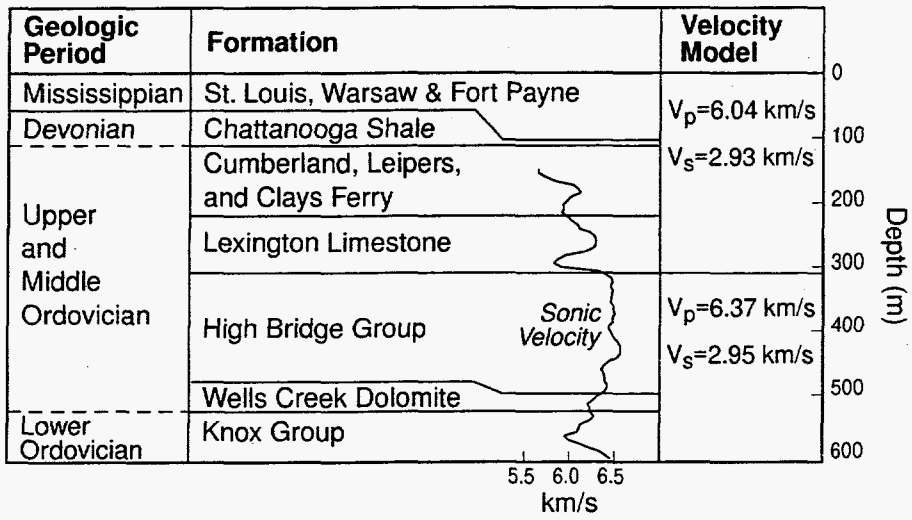
Geologic Period
Formation
Velocity Model
Mississippian
St. Louis, Warsaw & Fort Payne
Devonian
Chattanooga Shale
Upper and Middle Ordovician
Cumberland, Leipers, and Clays Ferry
Lexington Limestone
High Bridge Group
Wells Creek Dolomite
Lower Ordovician
Knox Group
Sonic Velocity
V_p=6.04 km/s
V_s=2.93 km/s
V_p=6.37 km/s
V_s=2.95 km/s
0
100
200
300
400
500
600
Depth (m)
5.5 6.0 6.5
km/s

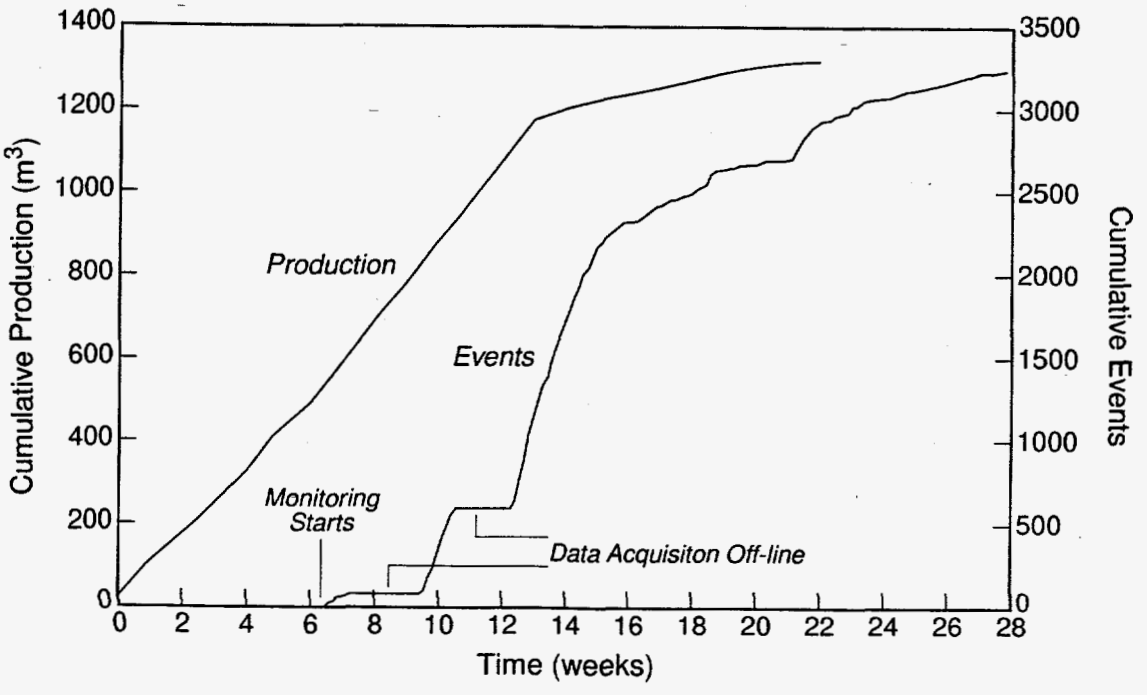
Cumulative Production (m3)
Cumulative Events
Time (weeks)
Production
Events
Monitoring Starts
Data Acquisiton Off-line
0
200
400
600
800
1000
1200
1400
500
1000
1500
2000
2500
3000
3500
0
2
4
6
8
10
12
14
16
18
20
22
24
26
28

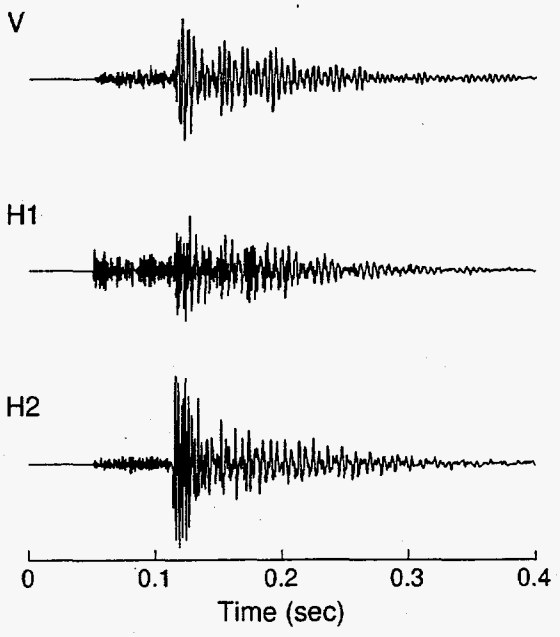
V
H1
H2
0
0.1
0.2
0.3
0.4
Time (sec)

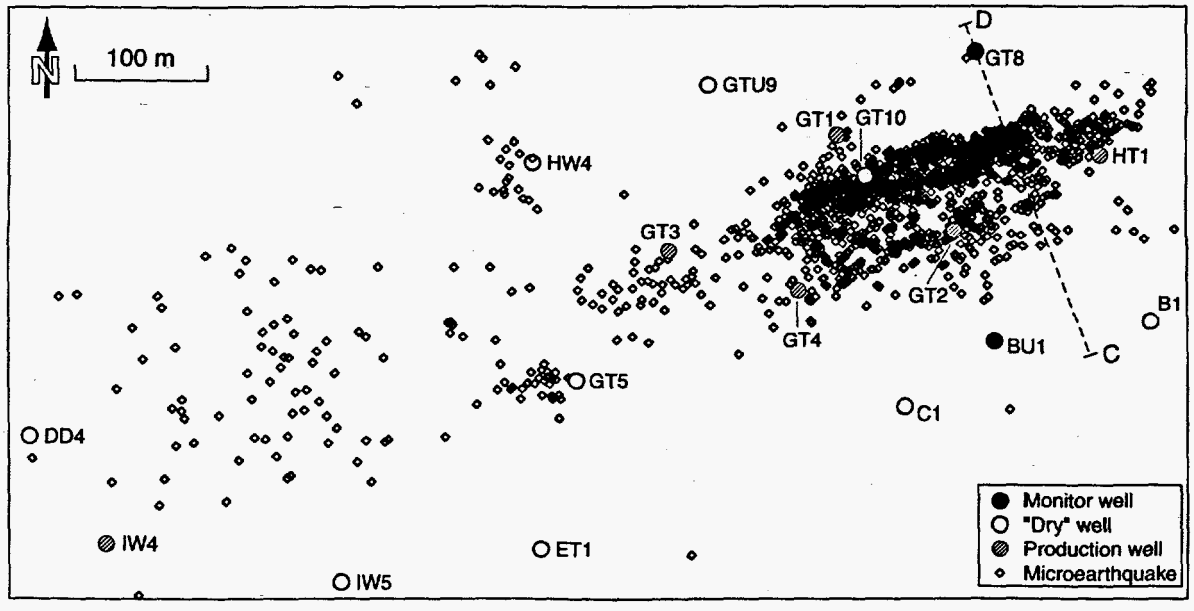
N
100 m
D
GT8
GTU9
GT1
GT10
HT1
HW4
GT3
GT2
B1
GT4
BU1
C
GT5
C1
DD4
IW4
ET1
IW5
Monitor well
"Dry" well
Production well
Microearthquake

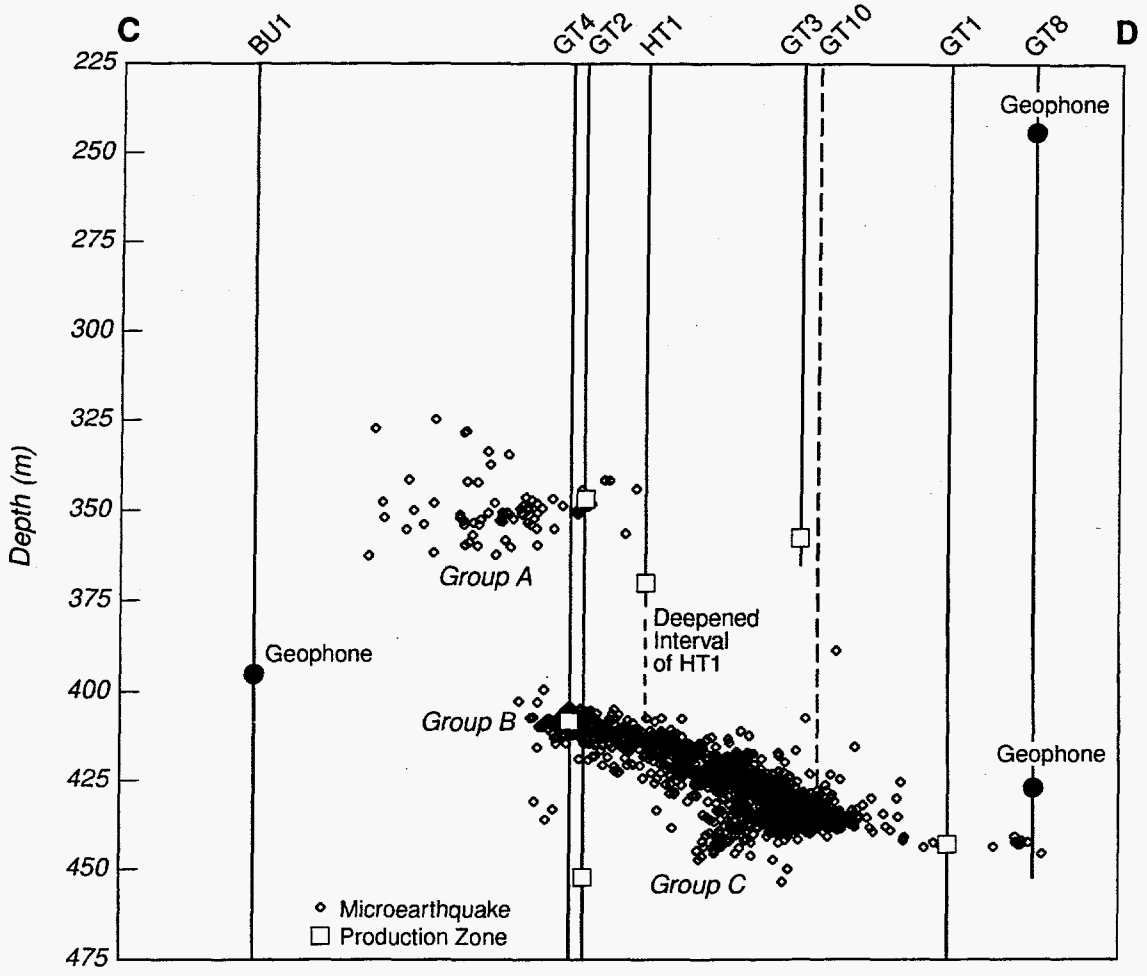
C
BU1
GT4
GT2
HT1
GT3
GT10
GT1
GT8
D
225
250
275
300
325
350
375
400
425
450
475
Depth (m)
Geophone
Group A
Deepened
Interval
of HT1
Geophone
Group B
Geophone
Group C
Microearthquake
Production Zone

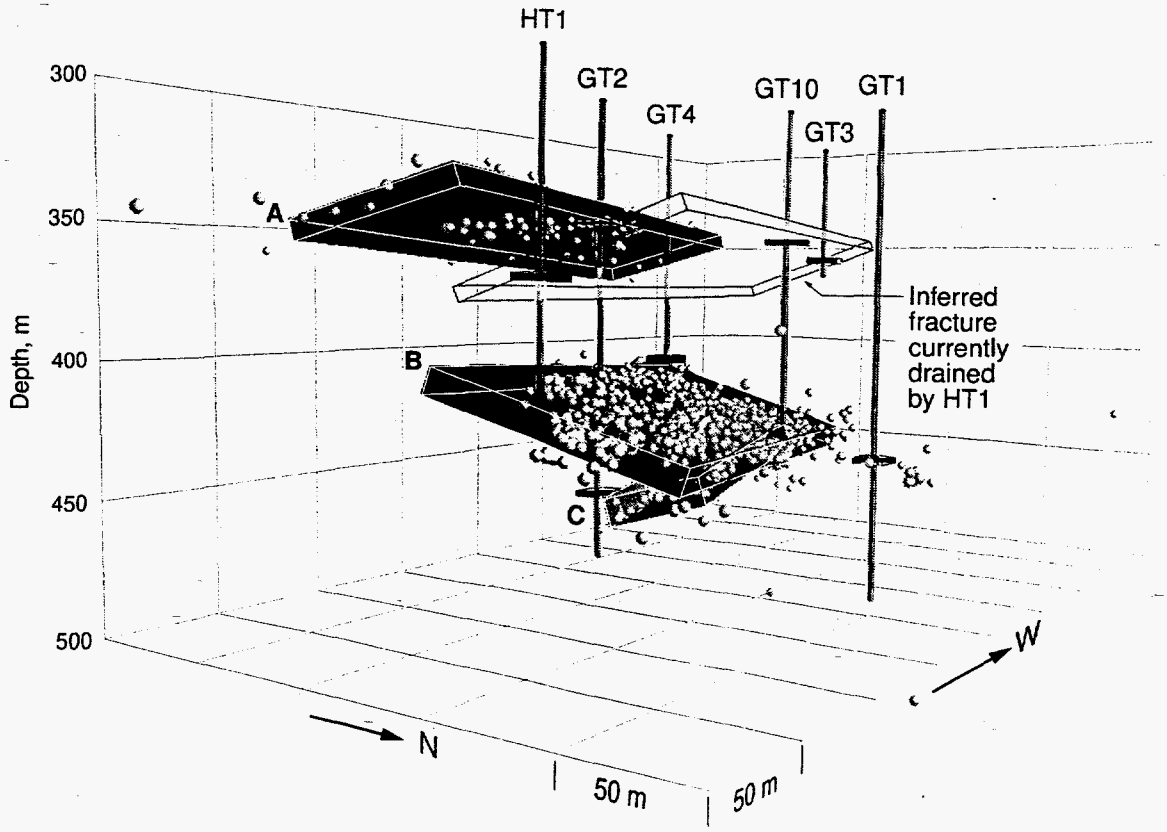
HT1
GT2
GT4
GT10
GT1
GT3
300
350
400
450
500
Depth, m
A
B
C
Inferred
fracture
currently
drained
by HT1
N
W
50 m
50 m

Summers Lease

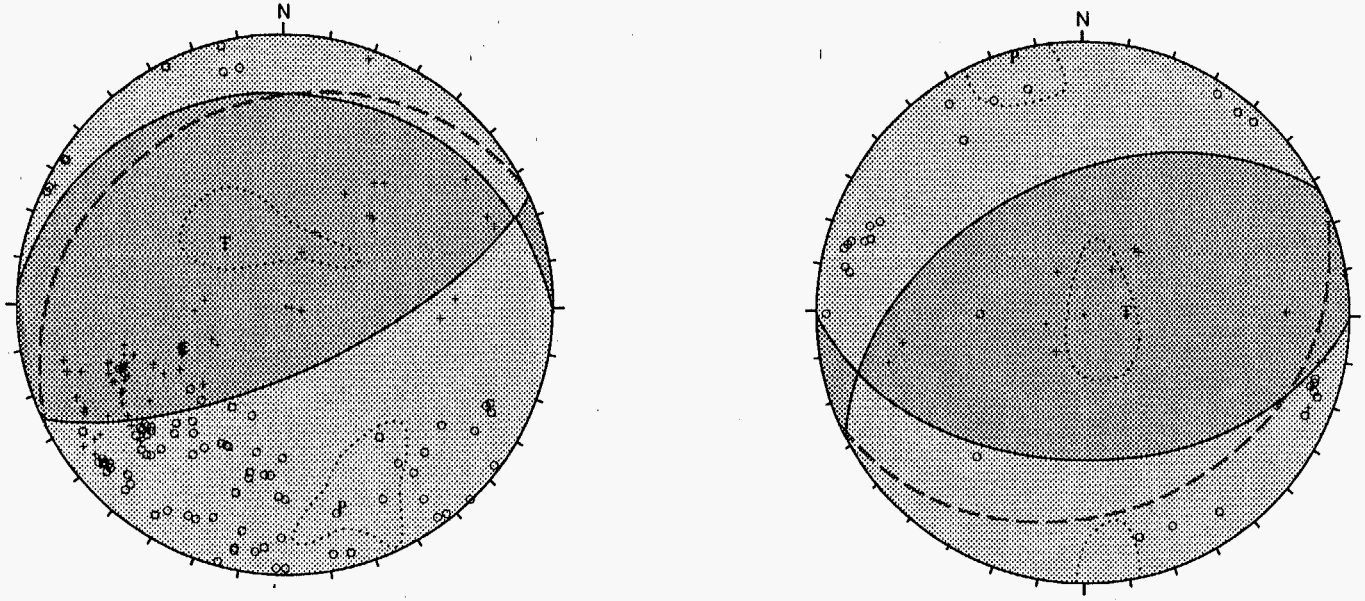

Tallent Lease